
This is an electronic reprint of the original article.
This reprint may differ from the original in pagination and typographic detail.

Vuorte, Maisa; Kuitunen, Susanna; Van Tassel, Paul R.; Sammalkorpi, Maria
Equilibrium state model for surfactants in oils: Colloidal assembly and adsorption

Published in:
Journal of Colloid and Interface Science

DOI:
[10.1016/j.jcis.2022.09.153](https://doi.org/10.1016/j.jcis.2022.09.153)

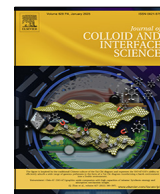
Published: 15/01/2023

Document Version
Publisher's PDF, also known as Version of record

Published under the following license:
CC BY

Please cite the original version:
Vuorte, M., Kuitunen, S., Van Tassel, P. R., & Sammalkorpi, M. (2023). Equilibrium state model for surfactants in oils: Colloidal assembly and adsorption. *Journal of Colloid and Interface Science*, 630, 783-794.
<https://doi.org/10.1016/j.jcis.2022.09.153>

This material is protected by copyright and other intellectual property rights, and duplication or sale of all or part of any of the repository collections is not permitted, except that material may be duplicated by you for your research use or educational purposes in electronic or print form. You must obtain permission for any other use. Electronic or print copies may not be offered, whether for sale or otherwise to anyone who is not an authorised user.



Equilibrium state model for surfactants in oils: Colloidal assembly and adsorption



Maisa Vuorte^{a,b}, Susanna Kuitunen^c, Paul R. Van Tassel^d, Maria Sammalkorpi^{a,b,e,*}

^a Department of Chemistry and Materials Science, School of Chemical Engineering, Aalto University, P.O. Box 16100, FI-00076 Aalto, Finland

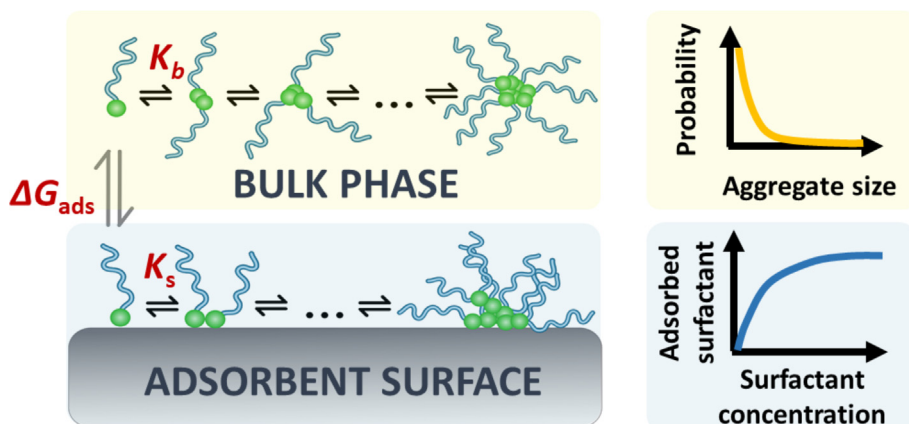
^b Academy of Finland Center of Excellence in Life-Inspired Hybrid Materials (LIBER), Aalto University, P.O. Box 16100, FI-00076 Aalto, Finland

^c Neste Oy, P.O. Box 310, FI-06101 Porvoo, Finland

^d Department of Chemical & Environmental Engineering, Yale University, New Haven, CT 06520, USA

^e Department of Bioproducts and Biosystems, School of Chemical Engineering, Aalto University, P.O. Box 16100, FI-00076 Aalto, Finland

GRAPHICAL ABSTRACT



ARTICLE INFO

Article history:

Received 13 April 2022

Revised 29 September 2022

Accepted 30 September 2022

Available online 10 October 2022

Keywords:

Adsorption

Aggregation

Self-assembly

Scaled particle theory

Colloids in oil

Reverse micelles

Surfactants

ABSTRACT

An equilibrium state model addressing the aggregation and adsorption of colloidal assemblies in apolar solvents (oils) via monomer exchange is presented. The model is based on the previously reported step-wise aggregation response of fatty acids and monoglycerides in bio-oils, and captures surface crowding via scaled particle theory (SPT). The sensitivity of key observables – mean aggregation number, adsorbed surfactant amount, and free monomer concentration – to model parameters is demonstrated. Fits to molecular modelling based aggregation and adsorption data of oleic acid and monoolein reveal that the model accurately reproduces chemically specific aggregate exponential distributions in both bulk and surface phases, even outside of its parameterization conditions. A biased state model, where the initial bulk aggregation step (dimer formation) differs from other steps results in a notable improvement in accuracy. Fits to various phospholipid adsorption isotherms demonstrate the applicability of the model to isotherm type experimental data. The fits reveal either monolayer or aggregate like adsorption structures, depending on surfactant head group charge. The presented model provides an easily accessible, computationally feasible means to estimate colloidal assembly and adsorption in oil environments, and enables assessment of surfactant aggregation propensity and adsorption energetics.

© 2022 The Authors. Published by Elsevier Inc. This is an open access article under the CC BY license (<http://creativecommons.org/licenses/by/4.0/>).

* Corresponding author at: Department of Chemistry and Materials Science, School of Chemical Engineering, Aalto University, P.O. Box 16100, FI-00076 Aalto, Finland.
E-mail address: maria.sammalkorpi@aalto.fi (M. Sammalkorpi).

1. Introduction

Adsorption of compounds from solution onto a solid surface is often used for separation and purification processes, and is central to many applications, including flotation [1–3], coatings [4–6], and lubricant technologies [7–9]. One important application is dry-washing, a non-destructive, adsorbent-based approach for purification and extraction of compounds from apolar solutions/ oils. Dry-washing is a promising purification method for, e.g., bio oils, due to its low cost, simplicity, and selectivity. While originally used to remove chlorophyll and pigments from bio oils, it can also be used for the selective adsorption of amphiphilic impurity species, such as, mono- and diglycerides [10], fatty acids [11–13], soaps [13], or phospholipids [14,15]. Common adsorbents for the process include, e.g., silicates, silica-based adsorbents, organo-clays, ion exchange resins, and activated carbon [10–12,14,16,17].

Previously, the kinetics and energetics of adsorption in bio oils on a variety of organo-clay, activated carbon, and mineral surfaces have been investigated using adsorption isotherms measured via quartz crystal micro balance (QCM) [18], interferometric surface force apparatus (SFA) [19,20], rheometry [21], colorimetry [22–25], and Fourier transform infrared spectroscopy (FT-IR) [26]. Furthermore, the structures formed at the oil – solid interface have been characterized using sum frequency spectroscopy (SFS) [27] and X-ray and neutron reflectometry [28–30]. The findings reveal that adsorption in vegetable oils occurs mainly via the functional groups of chemical species. In addition to adsorbing impurities, the polar ester groups typically found in triglycerides – the major component of most vegetable oils – promote their competitive adsorption on surfaces [18,19,23]. Adsorption strength and adsorption capacity is largely determined by hydrogen bonding [18,19,22,31]. Adsorption corresponding to monolayer coverage with both perpendicular and parallel molecular orientations depending on molecule chemistry, particularly the sterics of the hydrophobic moieties, have been observed [19,27,30,32]. Adsorption is also affected by the effect of moisture and wetting of the surface. Furthermore, the mono- and multilayer adsorption structures observed in dry solvent environments are disturbed by the presence of trace water [33]. Additional wetting has also been reported to increase the aggregate structures present at the adsorbent surface [33].

Molecular modelling approaches can provide highly complementary, molecular level information on surfactant adsorption processes. Recent efforts via classical molecular dynamics (MD) have focused on adsorption at the oil – solid interface, and have helped clarify the effects of surfactant structure [31,34], adsorbent chemistry and wetting [31,35], small polar impurities in the oil, e.g., water [36,37], and external forces, e.g., shear [8,36–38], on aggregate or film morphology and adsorption geometry. Additionally, Monte Carlo (MC) based approaches have been used to assess the effects of adsorbent e.g., heterogeneity [39], micellization propensity [40–42], and surfactant – surface interaction strength [42–44] on the adsorption of simple surfactant models.

An important contribution to the adsorption of bio-oils arises from intermolecular interactions between adsorbates, particularly in the form of spontaneous self-assembly [18,45–49]. While most bio oils have triglycerides as their majority molecular component, they also contain a diverse range of amphiphilic compounds; the precise composition of which depends on oil feedstock and processing methods [50–55]. Most naturally present amphiphilic compounds in bio-oils consist of one or more hydrophobic hydrocarbon tails connected by a significantly smaller hydrophilic head group. The head group can be either non-ionic (e.g., monoglycerides) or carry a net charge (e.g., phospholipids). In an apolar solution, these amphiphilic surfactant species self-assemble into reverse micelle-

like aggregates, with a hydrophilic core surrounded by a hydrophobic corona [31,56–62]. The self-assembly of surfactants in apolar solvents differs from that of typical aqueous surfactant solutions: in apolar bio-oil like environments, both monoglycerides and fatty acids exhibit a step-wise aggregation regime which results in an exponential aggregate size distribution [58,31]. Additionally, surfactants with significant hydrogen bonding capability, such as monoglycerides or phospholipids, can deviate from an exponential size distribution by showing preference to a given aggregate size regime. Such biased aggregation appears especially at higher surfactant concentrations, where larger aggregates are favoured [58,31]. For example, phospholipids – a strongly aggregating surfactant – self-assemble first to cylindrical aggregates and then undergo a further morphological change to spherical reverse micelles with increased phospholipid concentration [63], increased temperature [64,65], or the presence of water or cosurfactant, such as fatty acid [64,45,66].

The aggregation and adsorption response can also be considered by theory and modelling. Ideally, thermodynamic and equilibrium state surfactant aggregation and adsorption models include hydrophobicity driven aggregation, solvent entropy, adsorbent – surfactant chemistry and molecular interactions, as well as the effect of surface heterogeneities (site specific adsorption energies) [67–71]. For polar, aqueous surfactant solutions, where physisorption is driven mainly by hydrophobic interaction, the effects of dimerization [72], aggregation [67,73–76], differences in surfactant orientation [77], and multi-species adsorption [78,79] on isotherm behaviour have been investigated. To our knowledge, comparable models for apolar solvents do not currently exist. This gap is significant, as readily available prediction and interpretation to adsorption from oils would aid in a number of applications, including oil purification, flotation, and lubrication.

To fill the gap, we propose and implement here an equilibrium state model for describing bulk aggregation and surface adsorption of surfactants in apolar solvent environments. We implement the model, parametrize it against MD-simulated aggregation and adsorption data of mono- and diglycerides from model vegetable oil [31], and assess its robustness and predictive ability. We also test the model performance against experimental data of phospholipid adsorption onto acid activated sepiolite (from rapeseed oil) [14], in particular assessing model sensitivity. For all examined cases, we extract chemically specific model parameters for generalization and comparison. The significance is a well-characterized, robust, aggregation and adsorption model for surfactants in apolar solvent environments - to our knowledge, comparable models do not currently exist despite the high technological relevance of both aggregation and adsorption from apolar media. The model is easily generalizable, and provides robust predictions for practical surfactant in oil adsorption systems.

2. Methods

The thermodynamic equilibrium state model for capturing surfactant aggregation and adsorption in apolar solvent consists of one part capturing bulk solution step-wise growth of aggregates, and another part describing aggregation on a comparatively more crowded adsorbent surface. For simplicity, adsorption is treated as a reversible process and surface heterogeneities including specific adsorption sites are disregarded. The bulk and surface aggregation processes are coupled via monomer exchange between the bulk and surface aggregation models, *i.e.* all adsorption and desorption takes place as monomers. A conceptual sketch of the reaction equilibria is provided as Fig. 1. The model employs as important

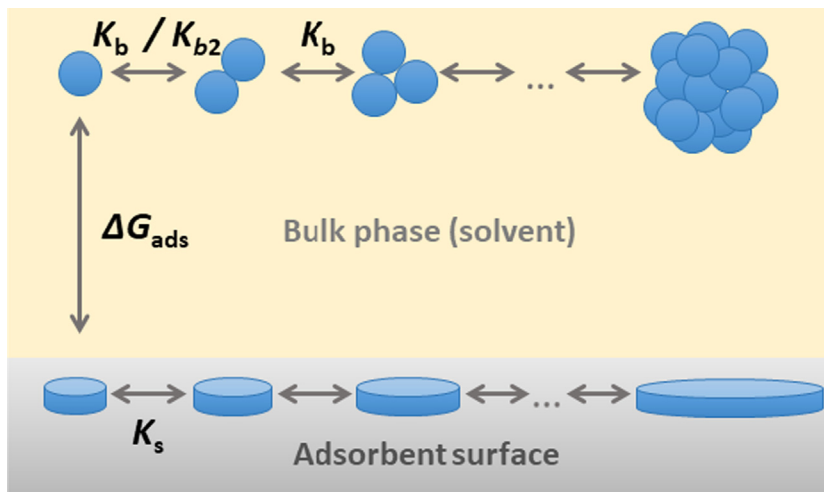


Fig. 1. Conceptual scheme of the aggregation and adsorption reaction equilibria considered by the state model. Parameters include bulk and surface monomer aggregation equilibrium coefficients K_b and K_s , and monomer free energy of adsorption ΔG_{ads} . Aggregation may be biased by separating K_b into a dimerization equilibrium constant K_{b2} differing in value from the equilibrium constant K_b corresponding to all assembly steps beyond dimerization, i.e. for aggregation number $n > 2$.

parameters the bulk and surface monomer aggregation equilibrium constants K_b and K_s , and also the free energy of monomer adsorption $\beta\Delta G_{\text{ads}}$, where $\beta = \frac{1}{k_b T}$, k_b is the Boltzmann constant, and T is the absolute temperature.

Following previous findings of stepwise aggregation for surfactants naturally present in plant oils and also cyclohexane type strongly apolar solvents [31,58], the model contains an assumption that the aggregation in bulk solution takes place via reversible stepwise monomer additions. Monomers can also adsorb onto the adsorbent surface, where they are treated as space filling hard discs. On the surface, monomers may further reversibly aggregate to form larger discs. We construct two models: in the simpler model, the same monomer equilibrium bulk aggregation constant K_b and surface aggregation constant K_s are employed for aggregates of all sizes. However, as the initial aggregation steps are prone to deviate from a stepwise exponential distribution [58], we also consider a model in which the dimerization step in bulk aggregation is governed by its own bulk aggregation equilibrium constant, K_{b2} , with all subsequent steps governed by K_b . This modification accounts for the bias in aggregate size that often arises from increased surfactant hydrogen bonding capability or head group charge [58,80,81], interplay of hydrocarbon tail sterics and head group [82], or the addition of small polar additives, such as water, to the oil [45,57,59,60,64,82–84]. For simplicity, surface aggregation is assumed to be less sensitive to the initial aggregation steps, i.e. same surface aggregation equilibrium constant K_s is used for all surface aggregation steps.

Aggregation within the bulk solution is described by an analytical solution to the aggregation model proposed by Vierros et al. [58]. The equilibrium constant K_b for dimer formation $2s_1 \rightleftharpoons s_2$ can be expressed as

$$K_b = \frac{[s_2]}{[s_1]^2}, \quad (1)$$

where $[s_1]$ and $[s_2]$ are the equilibrium bulk concentrations of monomers and dimers, respectively. Let $[s_n]$ then denote the concentration of aggregates with aggregation number n . Hence, $[s_1] = c_1$ and $[s_n] = c_n/n$, where c_n is the concentration of monomers in an aggregate of size n . We generalize the expression of K_b for bulk aggregation reaction $s_1 + s_{n-1} \rightleftharpoons s_n$ as

$$K_b^{n-1} = \frac{c_n}{nc_1^n}. \quad (2)$$

Total bulk monomer concentration c_{bulk} is then given by

$$\begin{aligned} c_{\text{bulk}} &= \sum_{n=1}^{n_{\text{max}}} c_n = c_1 + c_1 \sum_{n=2}^{n_{\text{max}}} n(c_1 K_b)^{n-1} = c_1 \sum_{n=1}^{n_{\text{max}}} n(c_1 K_b)^{n-1} \\ &= c_1 \frac{1 - (n_{\text{max}}+1)(c_1 K_b)^{n_{\text{max}}} + n_{\text{max}}(c_1 K_b)^{n_{\text{max}}+1}}{(1 - c_1 K_b)^2}, \end{aligned} \quad (3)$$

where n_{max} is the maximum aggregate size.

The formulation above treats the assembly steps as being thermodynamically equal for all n . Alternatively, as the dimerization equilibrium quite often differs from that of the following monomer addition steps, an explicit equilibrium constant K_{b2} may be introduced to describe the dimerization reaction $2s_1 \rightleftharpoons s_2$. In this case, K_{b2} is used merely for the dimerization step and a separate K_b is introduced as the equilibrium constant for all consecutive aggregation reaction steps beyond dimer formation, $s_1 + s_{n-1} \rightleftharpoons s_n$ for $n > 2$. Following the notation of Eq. 2, K_{b2} and K_b can be expressed as

$$K_{b2} = \frac{c_2}{2c_1^2} \quad (4)$$

$$K_b^{n-2} = \frac{c_n}{nK_{b2}c_1^n}. \quad (5)$$

This definition of K_{b2} and K_b leads to an overall surfactant concentration

$$\begin{aligned} c_{\text{bulk}} &= \sum_{n=1}^{n_{\text{max}}} c_n = c_1 + \sum_{n=2}^{n_{\text{max}}} nK_{b2}K_b^{n-2}c_1^n = c_1 \left(1 - \frac{K_{b2}}{K_b}\right) + \frac{c_1 K_{b2}}{K_b} \sum_{n=1}^{n_{\text{max}}} n(c_1 K_b)^{n-1} \\ &= c_1 \left(1 - \frac{K_{b2}}{K_b}\right) + \left(\frac{c_1 K_{b2}}{K_b}\right) \left(\frac{1 - (n_{\text{max}}+1)(c_1 K_b)^{n_{\text{max}}} + n_{\text{max}}(c_1 K_b)^{n_{\text{max}}+1}}{(1 - c_1 K_b)^2}\right). \end{aligned} \quad (6)$$

Eq. 6 simplifies to Eq. 3 when $K_{b2} = K_b$.

We assume that the adsorbent surface is more crowded than the bulk solution. Although the concentrations of bulk phase surfactants in apolar solvent environments are generally low, the significantly enhanced concentrations typically occurring at the surface suggests that accurate modelling of the adsorbed phase is important. Here, we assume the adsorbed aggregates to be hard disks, and employ scaled-particle theory to determine thermodynamic properties. Scaled Particle Theory (SPT) [85] has previously been widely used to describe thermodynamic equilibria of adsorption problems, including binary mixture [86], small molecule [87], and protein adsorption [88,89].

On the adsorbent surface, aggregates of size n are treated as space occupying hard discs of radius $R_n = an^{1/2}$, where a is a fitted constant. In this work, based on fitting to aggregate geometries for palmitic acid and monopalmitin in Ref. [58], we use parameter values $a = 0.201 \pm 0.008$ nm ($R^2 = 0.994$) for oleic acid and $a = 0.353 \pm 0.016$ nm ($R^2 = 0.992$) for monoolein. The surface aggregates are treated as a hard disc mixture, with disc–disc interactions defined by a pair potential $u(r_{ij})$:

$$u(r_{ij}) = +\infty \quad (0 \leq r_{ij} < \sigma_{ij})$$

$$= 0 \quad (r_{ij} \geq \sigma_{ij}) \quad (7)$$

where σ_{ij} is the collision radius of the discs. Here, $\sigma_{ij} = R_i + R_j$, where R_i and R_j are the radii of the interacting discs. The discs (aggregates) are not allowed to overlap on the adsorbent surface, which imposes an upper limit on their number density.

SPT is based on the reversible isothermal work $W(R)$ needed to expel all discs from a circular cavity of radius R at a given surface occupancy. A Boltzmann factor relates $W(R)$ to the probability $P_0(R)$ of finding a circular cavity of radius R free from any portion of any disc

$$P_0(R) = \exp[-\beta W(R)] \quad (8)$$

where k_B is the Boltzmann constant, and T the absolute temperature.

Our approach is similar to that used by Brusatori and Van Tassel [88] to describe protein adsorption from a binary mixture. However, here we extend the SPT treatment to account for n_{max} differently sized discs and to describing surfactant aggregation and adsorption in oils. To formulate the appropriate SPT approach, we begin with the exact value of $W(R)$ for $R \leq 0$:

$$\beta W(R \leq 0) = -\ln[1 - \pi \sum_{n=1}^{n_{max}} (R + R_n)^2 \rho_n] \quad (9)$$

where R_n is the radius of the disc corresponding to an aggregate of size n and ρ_n is the surface number density of the discs of that size. Eq. 9 results from the fact that a cavity with $R \leq 0$ can be blocked by at most one disc. For $R > 0$, we use a Taylor series expansion for $W(R)$:

$$\beta W(R) = \beta W(0) + \beta W'(0)R + \beta p \pi R^2$$

$$= -\ln[1 - \pi \sum_{n=1}^{n_{max}} R_n^2 \rho_n] + [2\pi(\sum_{n=1}^{n_{max}} \rho_n R_n)R / (1 - \pi \sum_{n=1}^{n_{max}} \rho_n R_n^2)]$$

$$+ \beta p \pi R^2 \quad (10)$$

where W' is the first order derivative of W with respect to R and p is the hard disk pressure of the 2D disk mixture. To derive p , we follow Brusatori and Van Tassel [88] in noting that the excess chemical potential μ_i^{ex} of disc of size R_i is equal to the reversible isothermal work of creating a cavity of size R_i , that is, $\mu_i^{ex} = W(R_i)$. Here, $\mu_i^{ex} = \mu_i - \mu_i^{ig}$, where μ_i^{ig} is the chemical potential of an ideal gas of species i . By employing the Gibbs–Duhem relation

$$\frac{\partial \beta p^{ex}}{\partial \rho_j} = \sum_{i=1}^{n_{max}} \rho_i \frac{\partial \beta \mu_i^{ex}}{\partial \rho_j} \quad (11)$$

to obtain the derivative of p^{ex} and then integrating the resulting equation with respect to ρ_j , the pressure term p is obtained:

$$\beta p = \sum_{n=1}^{n_{max}} \rho_n / (1 - \pi \sum_{n=1}^{n_{max}} \rho_n R_n^2) + \pi (\sum_{n=1}^{n_{max}} \rho_n R_n)^2 / (1 - \pi \sum_{n=1}^{n_{max}} \rho_n R_n^2)^2 \quad (12)$$

Now, Φ_n is defined as the probability of finding a cavity of size R_n , that is, $\Phi_n = P_0(R_n) = \exp(-\beta W(R_n))$. Assuming stepwise aggregate

growth on the adsorbent surface, in analogy to Eq. 2, the equilibrium constant expression becomes

$$K_s^{(n-1)} = \frac{\rho_n}{n(\frac{\rho_1}{\Phi_1})^n} \quad (13)$$

where K_s is the equilibrium constant for monomer surface aggregation.

To couple bulk with surface aggregation, a condition on the monomer chemical potential $\mu_1^{bulk} = \mu_1^{surface}$ is imposed, leading to

$$\ln\left(\frac{\rho_1}{\Phi_1}\right) + \beta \Delta G_{ads} = \ln(c_1) \quad (14)$$

where $\beta \Delta G_{ads}$ is the monomer change in free energy of adsorption. Previously, we have calculated comparable free energies of adsorption for fatty acids, monoglycerides, and phospholipids from model vegetable oil solutions using molecular dynamics simulations [31]. Such data can potentially be utilized for model fitting to comparable systems.

Combining Eqs. 13 and 14, and limiting the total number of surfactant monomers in the system to N_{tot} to give a closed solution, leads to the following set of non-linear equations:

$$\begin{cases} \left(\frac{\rho_1 K_s}{\Phi_1}\right)^n \Phi_n - \rho_n = 0 & (a) \\ \ln\left(\frac{\rho_1}{\Phi_1}\right) + \beta \Delta G_{ads} - \ln(c_1) = 0 & (b) \\ N_{tot} - \sum_{n=1}^{n_{max}} n \rho_n A - \sum_{n=1}^{n_{max}} c_n V = 0 & (c) \end{cases} \quad (15)$$

where A is the total adsorbent surface area, and V is the bulk solution volume.

For practical use of the model, we note that the total adsorbent area A and bulk solution volume V , and specifically the ratio A/V , are system dependent constants. The three main parameters of the model, $\beta \Delta G_{ads}$, K_b , and K_s , are system independent and can be obtained by, e.g. fitting to existing data points from other, but related systems. Additionally, the aggregate radius R_n should be matched with surfactant type, that is, fit to surfactant and aggregate structural data, such as radius of gyration.

The above set of non-linear equations of Eq. 15 is solved for $\rho_1, \rho_2, \dots, \rho_n$ and c_1 using a trust-region-dogleg equation solving algorithm. Penalty functions are applied to imaginary and negative solution roots to steer the solver towards positive and real roots. The concentrations c_2, c_3, \dots, c_n are subsequently calculated based on Eq. 2, or Eqs. 4 and 5, depending on the model. A genetic algorithm was used for parameter fitting and is detailed in Supplementary Information.

3. Results and discussion

First, we examine the sensitivity of the proposed adsorption model to variation of $\beta \Delta G_{ads}$, K_b , or K_s . The purpose is to map robustness ranges of the aggregation and adsorption responses for a variety of surfactant species, solvents and adsorbates. Fig. 2a presents the average bulk (solid lines) and surface (dashed lines) aggregation number when each of the three parameters is varied, while keeping the two other parameters constant. Correspondingly, in Fig. 2b, c, and d, the surface concentration of adsorbed surfactant and bulk concentration of total surfactant and free monomer at equilibrium are presented.

Data of Fig. 2a show that the average surface aggregate size responds strongly to K_s increasing from zero, i.e. stronger aggregation propensity at the surface. Increasing the adsorption free energy of the monomers $\beta \Delta G_{ads}$ elicits a similar sigmoidal response in increase surface aggregate size.

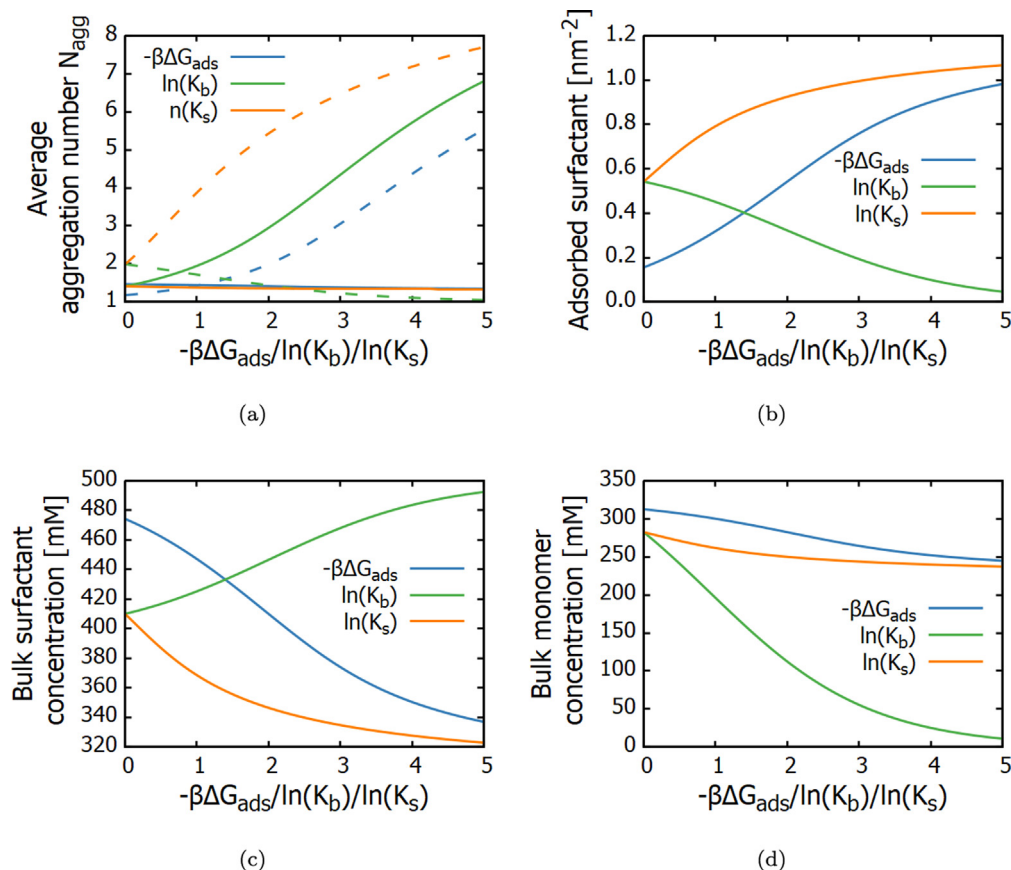


Fig. 2. Effect of bulk and surface aggregation equilibrium constants K_b and K_s , and monomer adsorption energy $\beta\Delta G_{\text{ads}}$ on modelled a) equilibrium aggregate size in bulk solution (solid lines) and on adsorbent surface (dashed lines), b) concentration of adsorbed surfactant, c) concentration of surfactant and d) free monomer in bulk phase at equilibrium. Dependency of K_b is mapped with keeping $\beta\Delta G_{\text{ads}} = -2.0$ and $K_s = 1.0$ constant, K_s with keeping $\beta\Delta G_{\text{ads}} = -2.0$ and $K_b = 1.0$ constant, and $\beta\Delta G_{\text{ads}}$ with keeping $K_b = 1.0$ and $K_s = 1.0$ constant. Initial bulk surfactant concentration is 0.5 M, surface area 100 nm^2 , and $R_n = 0.5(n)^{0.5}$.

The saturation of the surface at high $\beta\Delta G_{\text{ads}}$ or K_s is observed in the amount of adsorbed surfactant in Fig. 2b. Surface saturation and extrapolation of the increasing average surface aggregate size curve leads to an adsorption setup corresponding to monolayer coverage on a completely crowded surface. Conversely, an increase in K_b results in a depletion of surfactant from the adsorbent surface and a reduction in average surface aggregate size towards only monomers remaining on the adsorbent surface.

For bulk aggregation response, the effect of the three model parameters is, as expected, reversed. In brief, the bulk aggregation response is dominated by K_b , with an increase in K_b corresponding to the formation of larger bulk aggregates. Now, however, as the bulk solution can be considered to be much more dilute in terms of assemblies than the surface (and indeed no volume exclusion effects are considered for the bulk solution phase here), the bulk solution does not become saturated by the surfactant aggregates. Instead, the assemblies become larger with increasing K_b and the bulk monomer concentration diminishes.

The monomer concentration data in Fig. 2d reveals that an increase in $\beta\Delta G_{\text{ads}}$, K_b , or K_s all decrease the free monomer concentration. For K_b , this is due to formation of larger aggregates, as we simultaneously observe an increase in overall bulk surfactant concentration (see Fig. 2c). The monomer concentration response to changes in both $\beta\Delta G_{\text{ads}}$ and K_s is linked to Eq. 14. Specifically, $\beta\Delta G_{\text{ads}}$ determines the partitioning of monomers between bulk and surface: a more negative $\beta\Delta G_{\text{ads}}$ value results in a smaller monomer bulk concentration as adsorption is more favorable. On the other hand, an increase in K_s drives the formation of larger surface aggregates. This results in depletion of monomers at surface.

Eq. 14 corrects for this depletion by partitioning more monomer from bulk to surface. Plateaus at large K_s or $\beta\Delta G_{\text{ads}}$ values correspond to surface saturation.

Let us next compare the predictions of the thermodynamic model with perhaps the most common theoretical means used to describe monolayer adsorption, the Langmuir isotherm [90,91]. The Langmuir model is a useful description for cases where adsorption occurs to well-defined, identical adsorption sites, e.g. chemisorption. The adsorbate is treated as an ideal gas under isothermal conditions, while the adsorbent is assumed to be composed of distinct adsorption sites, each identical [92–94]. The adsorption phenomenon is a binding equilibrium reaction, where a free adsorbent species, here a surfactant monomer s_1 , binds with a surface adsorption site A to produce a bound adsorbate–adsorbent complex $A \cdot s_1$:



Let K_1 be the equilibrium constant for the Langmuir model binding reaction of Eq. 16. Surface coverage θ as a function of free surfactant monomer at equilibrium c_1 is then defined as

$$\theta = \frac{K_1 c_1}{1 + K_1 c_1} \quad (17)$$

In the model, surface coverage θ is one at monolayer saturation. Here, we define this Langmuir model upper limit based on hexagonal 2D packing of identical monomer sized discs. This leads to a maximum fractional surface coverage of $\theta = \pi\sqrt{3}/6$, independent of monomer disc size. Following the Langmuir model, K_1 can be calculated directly from $\beta\Delta G_{\text{ads}}$ within the model. The two main

assumptions of the Langmuir model are ideal smoothness of the adsorbent surface (all adsorption sites are equal) and the neglect of lateral adsorbate–adsorbate interactions, such as aggregation. An extension of the Langmuir model, the Moreau isotherm [95] includes an adsorbate–adsorbate interaction term I with surface coverage θ defined as:

$$\theta = \frac{K_m c_1 + I(K_m c_1)^2}{1 + 2K_m c_1 + I(K_m c_1)^2}, \quad (18)$$

where K_m be the equilibrium constant for binding at infinite dilution. The adsorbate–adsorbate interaction parameter I describes the attractive ($I > 1$) or repulsive ($0 < I < 1$) interaction between adsorbates on the surface. The Moreau isotherm reduces to the Langmuir isotherm when $I = 1$.

A comparison of surface coverage by the implemented non-biased aggregation model to the Langmuir and Moreau adsorption isotherms is presented in Fig. 3. To limit bulk aggregation, in the comparison with the Langmuir model, $K_b = 0.001$. The data reveal that an increased surface aggregation propensity, that is, an increase in K_s results in a more crowded surface. However, significant surface aggregation is required for the proposed thermodynamic model to predict similar degree of surface coverage as predicted by the Langmuir model. This is expected as Langmuir greatly underestimates the crowding of real surfaces, as it assumes the filling of independent sites. This surface crowding can be accounted to some extent by the Moreau isotherm via introducing a repulsive term between adsorbates, see Eq. 18. Therefore, at $K_s = 0$, where only monomers adsorb, our SPT-based model predicts much lower surface coverage than the Langmuir model, but roughly comparable surface coverage to a Moreau model with a high repulsive parameter. At higher K_s , larger aggregates may exist in the SPT-based model which leads to the equilibrium being shifted toward higher coverage.

Next we demonstrate the model parameterization for a chemically specific molecular system, and assess the performance of the model for specific, existing data sets. First, we take MD simulated bulk aggregate and adsorbed aggregate distributions for oleic acid and monoolein in triolein and adsorbed on a quartz or cristobalite surface. The aggregate distributions have been originally published in Ref. [31]. The parameters were fitted by the genetic algorithm protocol described in Supplementary Information. Fig. 4 plots the original and fitted bulk and surface aggregate distributions for oleic acid on quartz and cristobalite. The fitted parameters correspond-

ing to the graph have been collected to Supplementary Information Table S1.

Altogether, the model predicts accurately the exponential aggregate distributions for both bulk aggregation phase and the aggregation occurring at the adsorbent surface. Additionally, it effectively captures the concentration dependent shift in the aggregate distributions. However, the fitted model appears to underestimate monomer surface concentration. This likely results from underestimation of $\beta\Delta G_{\text{ads}}$. $\beta\Delta G_{\text{ads}}$ largely determines the partitioning of surfactant between the bulk phase and the surface due to coupling of the bulk and surface aggregation models via monomer chemical potential, see Eq. 14. Additionally, we note that the MD-simulated distributions are subject to simulation time (here 500 ns, *i.e.* very long) and finite-size effects [31]. These likely result in the decrease in fitted $\beta\Delta G_{\text{ads}}$ and K_b with concentration for oleic acid on quartz or cristobalite in Table S1 in Supplementary Information.

The aggregates on the adsorbent surface are currently treated as circular discs. In anhydrous conditions, both monoglycerides and fatty acids form filament-like aggregates in oil, that is, one aggregate dimension is significantly elongated in comparison to the other two [31,58,59]. Regardless, the assumption of circular aggregates made in this work provides a good fit to fatty acid aggregation data. This observation is unexpected, likely rising from some cancellation of errors, as flexible filaments could be expected to deviate in their adsorption response from circle-like disks significantly.

Fitting of the model to 15 wt-% oleic acid data from the MD simulations enables us to extrapolate the mean aggregate size at also other concentrations, see Fig. 5. The predicted average aggregate size closely matches the data of the MD simulations from Ref. [31]. However, the monomer concentrations have mismatch. At sufficiently high concentrations, the mismatch in monomer partitioning leads to over estimation of the mean aggregate size. Altogether, the data of Fig. 5 show that the presented model extrapolates well to concentrations outside its parametrization concentration.

As shown by data in Fig. 4, the model that has a single bulk aggregation equilibrium constant (see Eqs. 2 and 3) produces a good fit to fatty acid data. Additionally, the assumptions of i) adsorption occurring as monomers, and ii) identical free energies of adsorption for free and aggregate monomers, lead to good agreement with data from apolar solvent solutions of surfactants with

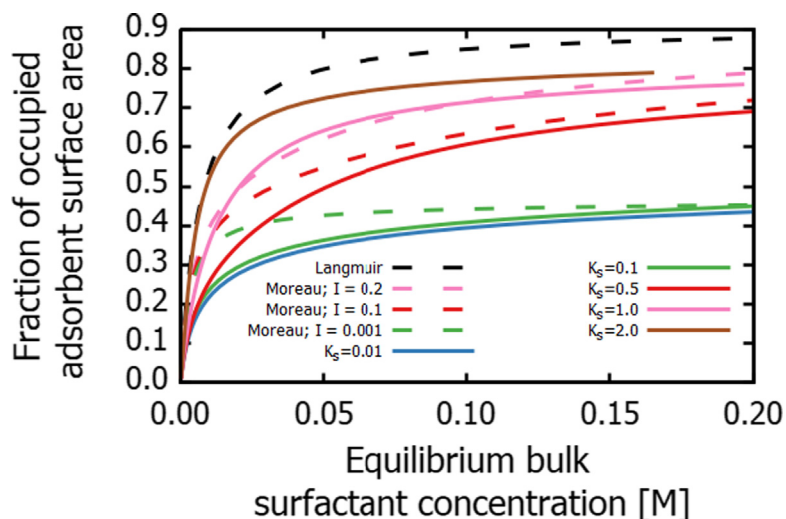


Fig. 3. Adsorption isotherms based on the non-biased adsorption model (solid lines) compared to prediction according to Langmuir and Moreau adsorption theory (dashed lines). The data is for $K_b = 0.001$ and $\beta\Delta G_{\text{ads}} = -5.0$. Surface area is 500 nm^2 and $R_n = 0.5n^{1/2} \text{ nm}$.

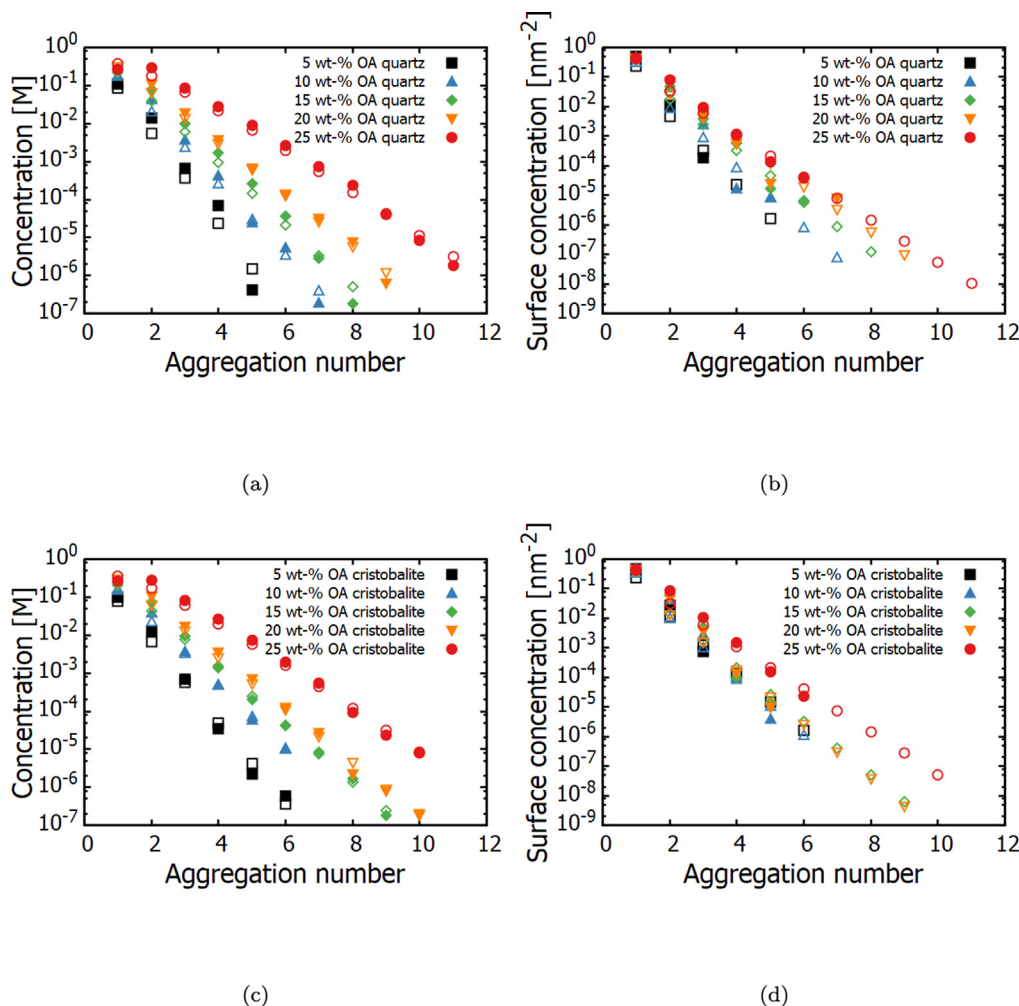


Fig. 4. The MD simulated (filled symbols) and fitted model (open symbols) aggregate distributions for oleic acid in triolein. Panel (a) presents the bulk and panel (b) the surface aggregate distributions on quartz. Corresponding distributions on cristobalite are presented in panel (c) for bulk and in panel (d) for surface aggregate distributions. MD simulations data originates from Ref. [31].

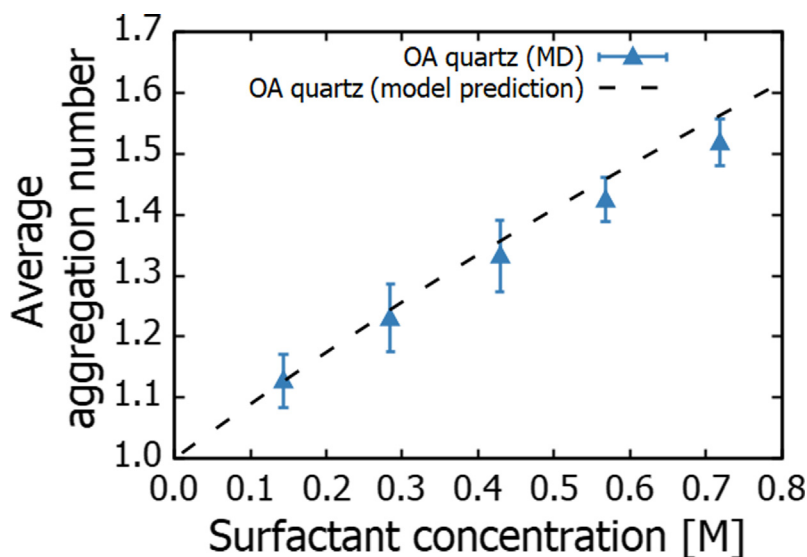


Fig. 5. The average bulk aggregate size predicted by the fitted thermodynamic model with a comparison to average aggregate sizes from MD simulations data originating from Ref. [31]. The MD simulations data rise from a variety of concentrations ranging between 5 wt-% to 25 wt-% initial bulk concentration of oleic acid while the fitted thermodynamic model prediction is based on the model fit to the 15 wt-% oleic acid MD data.

relatively small polar head group and limited hydrogen bonding capability, *i.e.* fatty acids. However, for surfactants with larger hydrophilic headgroups (and increased hydrogen bonding capability) or surfactants with charged groups (*e.g.* fatty acid soaps or phospholipids), an aggregation bias towards specific aggregate size exists [31,58,81,96]. Similar effect arises from water dispersed in bio oils as surfactant headgroup hydration leads to formation of water bridges and aqueous cores in surfactant reverse micelles and other aggregates [45,57,59,61,97–100]. Although a simplification, the biased aggregation model where dimer formation is differentiated from other bulk aggregation steps, as defined by Eqs. 4 and 5, captures the essence of this bias.

The monoolein data set of Ref. [31] is an example of such enhanced aggregation propensity due to increased surfactant head group hydrogen bonding capability. This also leads to a stronger binding to the adsorbent surface in comparison to oleic acid. Indeed, this is reflected in larger K_b and $\beta\Delta G_{ads}$ values, see Table S1 in Supplementary Information, in the fit to MD data. Additionally, at higher monoglyceride concentrations, larger surfactant aggregates become thermodynamically more favoured compared to initial aggregation steps [58,31,59]. In the thermodynamic model parameter fit (Table S1), this shows as a strong concentration dependency of K_b for monoolein.

To account for aggregation energy differences between initial aggregation steps (dimerization) and later aggregation steps, we include also an explicit dimerization constant K_{b2} that may differ from the bulk aggregation equilibrium constant K_b for later aggregation steps ($n > 2$). The equilibrium constants K_{b2} and K_b are defined in Eqs. 4 and 5. Let us next fit this biased aggregation model to the monoolein aggregate distributions. The fitted K_{b2} , K_b , K_s , and $\beta\Delta G_{ads}$ values are presented in Supplementary Information in Table S2. Fig. 6 plots the fit of the biased model to the MD simulations data for 10 wt.% concentration of monoglyceride in triolein solvent and adsorbing on quartz. Notably, the fitting results in a lower K_{b2} compared to K_b . This means that the initial dimerization is significantly less thermodynamically favoured than subsequent growth steps. A similar bias has previously been noted by Vierros et al. [58]. In the current fit, each point in the MD-simulated aggregate distribution is weighted equally. For a better fit, uneven weights could be applied to better account for the scatter at the large aggregate end of the distribution, see especially Fig. 6a); in the current fit, this scatter in original data set leads to a significant underestimation of both bulk

monomer concentration and small surface aggregate concentrations.

Indeed, individually tuned weights for different aggregation steps would bring access to additional resolution in terms of chemical specificity of the modelled system. However, this route is at the cost of simplicity and leads to more complex, parameterization data heavy solutions. Additionally, creating such complex models does not guarantee improved interpretability.

To further generalize the model for surfactants with larger polar headgroups, we next demonstrate the performance and fitting of the model to phospholipid adsorption isotherm data for DOPC, DOPA-HNa, and DOPA-H₂ in rapeseed oil on acid activated sepiolite. The isotherm data measured by inductively coupled plasma spectrometer were originally published by Laatikainen et al. in Ref. [14]. The residual water content of 0.2 wt.% in the measured system is expected to promote aggregation of the phospholipids when bound to the polar headgroups although the level of hydration depends on phospholipid type. At low phospholipid concentrations (~ 0.5 mmol/kg), that are well below the experimentally observed CMCs [101], water content between 0.03 and 1.00 wt.% was reported to have minimal effect on overall adsorption [14]. While the existence of CMC for surfactants in apolar solvents is debatable [31,58,102], it is well known that water, as well as phospholipid composition and solvent medium influence the aggregation propensity and reverse micelle morphology of phospholipids [45,64,66]. Here, step-wise growth of bulk phospholipid aggregates is assumed with no present CMC. We note that while evidence of step-wise aggregate growth exists for weakly polar surfactants such as fatty acids and monoglycerides [31,58,102], evidence of similar aggregate growth for charged surfactants, such as phospholipids, remains sparse in current literature [103]. Due to both low phospholipid concentration and low hydration of the phospholipid heads, we choose the simplified model with one bulk aggregation equilibrium constant as the comparison model. For the fit, a surface area of 176 m²/g for the acid activated sepiolite is assumed [14]. In addition to ΔG_{ads} and K_b , a radius r to describe average molecular area is also fitted. As phospholipids are expected to adsorb as monolayers at hydrophilic solid - liquid interfaces in apolar solvents [14,104], no aggregation at adsorbent surface is included in the fitted model, *i.e.* K_s is set to zero.

The original data by Laatikainen et al. and our model fits are presented in Fig. 7a. The fitted values for ΔG_{ads} , K_b , and r are as follows: $\beta\Delta G_{ads} = -13.31$ ($\simeq -37.43$ kJ/mol), $K_b = 9.68$, and $r = 0.47$

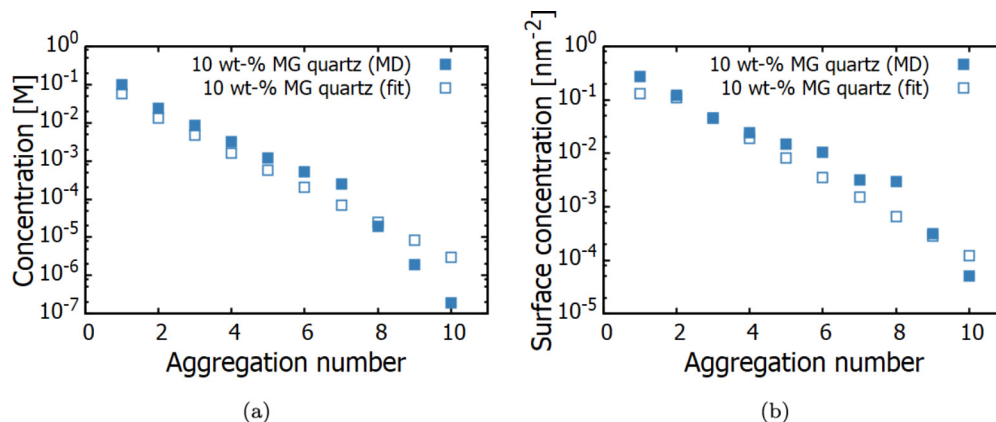


Fig. 6. Aggregate size distribution (a) in bulk solution and (b) on surface for 10 wt.% monoolein in triolein on quartz as predicted by MD-simulations and fitted model with explicit K_{b2} and K_b .

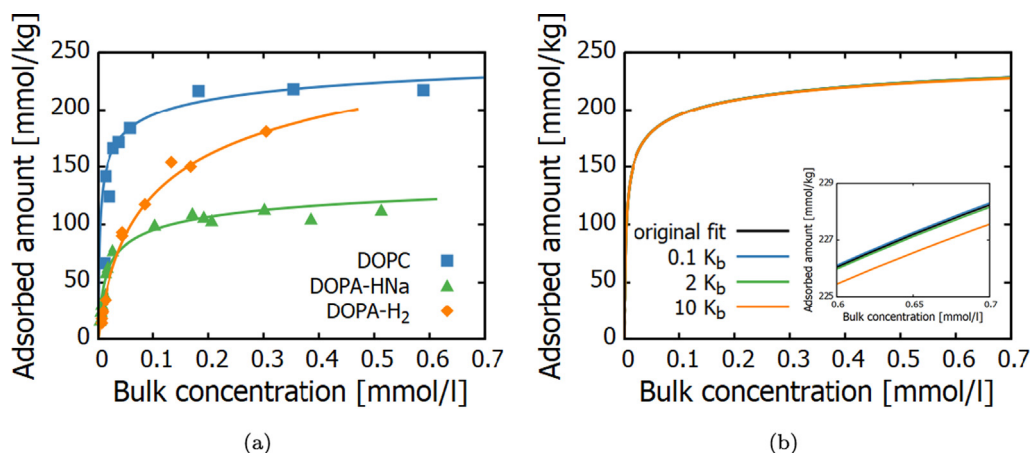


Fig. 7. (a) Adsorption isotherms (bulk equilibrium concentration vs. adsorbed surfactant per kg of clay) for DOPC, DOPA-HNa and DOPA-H₂ from rapeseed oil onto acid-activated sepiolite at $T = 65^\circ\text{C}$, and water content of 0.2 wt-%. Filled symbols denote the experimental isotherm data originally published by Laatikainen et al. [14], solid lines show the fitted model isotherm prediction. (b) Fitted adsorption isotherm for DOPC plotted using different values of K_b .

nm for DOPC, $\beta\Delta G_{\text{ads}} = -11.13$ (≈ -31.28 kJ/mol), $K_b = 6.62$, and $r = 0.60$ nm for DOPA-HNa, and $\beta\Delta G_{\text{ads}} = -9.97$ (≈ -28.04 kJ/mol), $K_b = 13.42$, and $r = 0.39$ nm for DOPA-H₂. Notably, the $\beta\Delta G_{\text{ads}}$ values resulting from our model fit are $\sim 4 - 11$ kJ/mol higher than those reported by Laatikainen et al. based on a Moreau isotherm fit to the adsorption isotherm data [14]. On the other hand, for DOPC and DOPA-HNa, the fitted r values fall between those reported by Laatikainen et al. [14] based on observed surface saturation and measured sepiolite surface area, and molecular surface areas based on packing of the respective phospholipids in a bilayer (0.46 nm for DOPC and 0.50 nm for DOPA-HNa) [105,106]. For DOPA-H₂, the fitted r value falls below that expected for bilayer-like packing (0.49 nm) [106]. We conclude from this that the packing of DOPC at saturation is close to that of a bilayer. On the other hand, the sparser packing of DOPA-HNa on the surface corresponds with the expected electrostatic repulsion of the charged head groups. Finally, for DOPA-H₂, the tighter packing suggests the presence of surface aggregates, even though surface aggregation was ignored in the current fit.

When no surface aggregation is included in the model, the choice of K_b has minimal effect on the amount of adsorbed surfactant at equilibrium. Instead, the partitioning of surfactant between bulk and surface is determined by $\beta\Delta G_{\text{ads}}$ while r determines the saturation concentration of the isotherm. The insensitivity of the isotherm is demonstrated in Fig. 7b, where the original fitted K_b value for DOPC is scaled by a factor of 0.1, 2, and 10 without significant changes to the predicted isotherm. The significance of this is that if the proposed model is fit to isotherm data, K_b can be considered as a free parameter.

The three main model parameters – $\beta\Delta G_{\text{ads}}$, K_b , and K_s – can be directly mapped to experimentally observable properties, specifically the free energy of adsorption and the free energy of micellization (or dimerization). The mismatch between experimentally determined free energies of adsorption – particularly when derived via isotherm fitting – and the model prediction can be significant as demonstrated here. Alternatively, molecular modelling techniques can be used to determine the adsorption energies of single surfactants [31,34,58,107,108] and free energies of aggregation [58,109–112]. Experimentally determined free energies of micellization [113–115] could also be mapped to K_b equilibrium constant. The value of K_s , that is, the aggregation propensity at the surface, is related to K_b and surfactant – surfactant interaction strength. Additionally, it is modified by the effects of surface diffusion and adsorption geometry of single surfactants and pre-aggregates.

While the model accurately replicates aggregation and adsorption regimes in the examined simple model systems, improvement prospects remain. First, while native concentrations of amphiphilic impurities in typical bio-oils are low, deviation from ideal mixture behaviour should be expected, especially for strongly hydrogen bonding or charged species, or in the presence of water. Such non-ideality could be accounted for by introducing activity-based correction factors to the model. Additionally, the SPT potential could be augmented by an additional Yukawa potential based term to account for electrostatic repulsion, which is relevant for adsorption of charged species, such as phospholipids or soaps. The adsorption of charged surfactant species is also sensitive to the presence of water [14,116], ions [14,117], and charged adsorbent surface moieties [34,101], which all contribute to the screening of electrostatic interactions and therefore packing of the surfactant at the interface. Additionally, surface morphology guides the packing [118,119]. Also the treatment of surface aggregates could be improved to better describe e.g., the rod- or filament-like aggregates [31,58–60] formed by species such as monoglycerides and fatty acids in anhydrous apolar solvents. We note, however, that despite the current model assuming circular disks, a relatively good fit is obtained for also such filament-like systems. Indeed, the SPT-based adsorption has been priorly modified for adsorption of particles of arbitrary shape [120]. However, the treatment of surface aggregates as two-dimensional space filling discs abstracts the three-dimensional packing of the surfactants. Particularly, the surfactant tail conformation changes upon adsorption can be significant, leading to an entropic contribution [119,121–123]. This is now omitted in the model. Finally, the adsorbent surface is assumed perfectly planar here and no information on surface roughness or preferential adsorption sites or conditions is included in the model. Advancements of the model could include considering the roughness and its effect on the adsorption for better match with real, non-ideal adsorbents. Another potential future extension of the model includes implementing a competing adsorbate species into the model, which would most likely capture better the behaviour of real oil systems, as well as provide insight into the diverse equilibrium phases based on e.g., the relative adsorption energies of the two competing adsorbates.

4. Conclusions

We presented and implemented an equilibrium state model for describing step-wise aggregation and adsorption of surfactants in apolar solvent environments. The model encompasses step-wise

bulk aggregation coupled with step-wise surface aggregation via monomer exchange between the bulk and the surface populations. Crowding of the surface is accounted for by an SPT approach. To account for a bias toward specific aggregate sizes in bulk or at the surface due to e.g., ionic groups, significant hydrogen bonding capability, head group hydration, or small polar additives in the apolar solvent environment, we also introduced as the simplest solution an explicit dimerization constant that may differ from the bulk aggregation constant used for the subsequent aggregation steps. We demonstrated the sensitivity and robustness of the models against variation of their parameters, and mapped the performance against both microscopically detailed simulations and experimental adsorption isotherm data of typical surfactants in bio-oils. The presented particle-level thermodynamic approach to describing colloidal assemblies and their adsorption response in low dielectric environments is, to our knowledge, a currently non-existing approach to predict equilibrium response of apolar solvent surfactant solutions. Most importantly, the approach overcomes the challenges associated with molecular level descriptions of such systems [124–126].

In summary, we presented here a model capable of predicting practical aggregation and adsorption behaviour in a set of technologically relevant bio-oil surfactant adsorption systems. The model can also be used to assess the likely adsorption structures based on the parameter values relating to surfactant chemistry, aggregation propensity, and adsorption strength. These parameters can be tuned to match specific chemical systems and experimentally accessible observables. For example, packing density on adsorbent surface, mean aggregate size, and variance can be extracted, as demonstrated by the fits to phospholipid adsorption data. Understanding of such surfactant equilibrium assemblies plays an important role in e.g., optimising sorption-based extraction and purification processes. Furthermore, bulk phase equilibrium aggregates may be linked to e.g., rheological properties of microemulsion systems. In total, the presented model brings access to equilibrium predictions and interpretation of the response of a wide variety of surfactant - apolar solvent - adsorbent systems.

Data availability

Data associated with the manuscript, including an implementation of the model, is available at <https://doi.org/10.23729/2f498581-d200-43ae-b3b0-8673f2fdf89d>.

Declaration of Competing Interest

The authors declare that they have no known competing financial interests or personal relationships that could have appeared to influence the work reported in this paper.

Acknowledgements

This work was partly financed by the Fortum and Neste Foundation project 20210130 and Academy of Finland through its Centres of Excellence Programme (2022–2029, LIBER) under project No. 346111. Computational resources by CSC IT Centre for Science, Finland, RAMI – RawMatTERS Finland Infrastructure, and Aalto Science-IT project are also gratefully acknowledged. M.S. is grateful for the support by the FinnCERES Materials Bioeconomy Ecosystem and use of the Bioeconomy Infrastructure at Aalto. We thank Dr. Markku Laatikainen and Prof. Tuomo Sainio for the raw data corresponding to Ref. [14] which enabled explicit comparison of the model to the experimental adsorption isotherms.

Appendix A. Supplementary material

Supplementary data associated with this article can be found, in the online version, at <https://doi.org/10.1016/j.jcis.2022.09.153>.

References

- [1] Y. Foucaud, M. Badawi, L. Filippov, I. Filippova, S. Lebègue, A review of atomistic simulation methods for surface physical-chemistry phenomena applied to froth flotation, *Miner. Eng.* 143 (2019) 106020.
- [2] J. Sokolović, S. Misković, The effect of particle size on coal flotation kinetics: A review, *Physicochem. Probl.* 54 (2018).
- [3] S. Paria, K.C. Khilar, A review on experimental studies of surfactant adsorption at the hydrophilic solid–water interface, *Adv. Colloid Interface Sci.* 110 (2004) 75–95.
- [4] S. Saraf, C.J. Neal, S. Das, S. Barkam, R. McCormack, S. Seal, Understanding the adsorption interface of polyelectrolyte coating on redox active nanoparticles using soft particle electrokinetics and its biological activity, *ACS Appl. Mater. Interfaces* 6 (2014) 5472–5482.
- [5] P.M. Claesson, E. Poptoshev, E. Blomberg, A. Dedinaite, Polyelectrolyte-mediated surface interactions, *Adv. Colloid Interface Sci.* 114 (2005) 173–187.
- [6] S. Llamas, E. Guzman, F. Ortega, N. Baghdadli, C. Cazeneuve, R.G. Rubio, G.S. Luengo, Adsorption of polyelectrolytes and polyelectrolytes-surfactant mixtures at surfaces: a physico-chemical approach to a cosmetic challenge, *Adv. Colloid Interface Sci.* 222 (2015) 461–487.
- [7] R.F. Apóstolo, G. Tsagkaropoulou, P.J. Camp, Molecular adsorption, self-assembly, and friction in lubricants, *J. Mol. Liq.* 277 (2019) 606–612.
- [8] M. Doig, C.P. Warrens, P.J. Camp, Structure and friction of stearic acid and oleic acid films adsorbed on iron oxide surfaces in squalane, *Langmuir* 30 (2014) 186–195.
- [9] J.P. Ewen, S.K. Kannam, B. Todd, D. Dini, Slip of alkanes confined between surfactant monolayers adsorbed on solid surfaces, *Langmuir* 34 (2018) 3864–3873.
- [10] V.A. Mazzieri, C.R. Vera, J.C. Yori, Adsorptive properties of silica gel for biodiesel refining, *Energy Fuels* 22 (2008) 4281–4284.
- [11] D.R. Taylor, C.B. Ungermann, Z. Demidowicz, The adsorption of fatty acids from vegetable oils with zeolites and bleaching clay/zeolite blends, *J. Am. Oil Chem. Soc.* 61 (1984) 1372–1379.
- [12] U. Kalapathy, A. Proctor, A new method for free fatty acid reduction in frying oil using silicate films produced from rice hull ash, *J. Am. Oil Chem. Soc.* 77 (2000) 593–598.
- [13] P. Assawaengrat, P. Jintanavasan, P. Kitchaiya, Adsorption of ffa, soap and glycerine in biodiesel using magnesium silicate, *Chem. Eng. Trans.* 43 (2015) 1135–1140.
- [14] M. Laatikainen, W. Srithammavut, B. Toukonniitty, I. Turunen, T. Sainio, Phospholipid adsorption from vegetable oils on acid-activated sepiolite, *Adsorption* 21 (2015) 409–417.
- [15] S.M. Silva, K.A. Sampaio, R. Ceriani, R. Verhe, C. Stevens, W. De Greyt, A.J.A. Meirelles, Adsorption of carotenes and phosphorus from palm oil onto acid activated bleaching earth: equilibrium, kinetics and thermodynamics, *J. Food Eng.* 118 (2013) 341–349.
- [16] A.B. Fadhil, M.M. Dheyab, A.Y. Abdul-Qader, Purification of biodiesel using activated carbons produced from spent tea waste, *J. Assoc. Arab Univ. Basic Appl. Sci.* 11 (2012) 45–49.
- [17] D.F. Stout, L.E. and Chamberlain, J.M. McKelvey, Factors influencing vegetable oil bleaching by adsorption, *J. Am. Oil Chem. Soc.* 26 (1949) 120–126.
- [18] K.O. Evans, G. Biresaw, Quartz crystal microbalance investigation of the structure of adsorbed soybean oil and methyl oleate onto steel surface, *Thin Solid Films* 519 (2010) 900–905.
- [19] A. Proctor, C. Adhikari, G.D. Blyholder, Lipid adsorption on commercial silica hydrogels from hexane and changes in triglyceride complexes with time, *J. Am. Oil Chem. Soc.* 73 (1996) 693–698.
- [20] S.M. Lundgren, M. Ruths, K. Danerlöv, K. Persson, Effects of unsaturation on film structure and friction of fatty acids in a model base oil, *J. Colloid Interface Sci.* 326 (2008) 530–536.
- [21] G. Biresaw, A. Adhikari, S. Erhan, C. Carriere, Friction and adsorption properties of normal and high-oleic soybean oils, *J. Am. Oil Chem. Soc.* 79 (2002) 53.
- [22] J. Mingyu, A. Proctor, The effect of added solvents on soy oil leucine adsorption by silicic acid, *J. Am. Oil Chem. Soc.* 70 (1993) 575–578.
- [23] H.G. Brown, H.E. Snyder, Adsorption of soy oil phospholipids on silica, *J. Am. Oil Chem. Soc.* 62 (1985) 753–756.
- [24] M. Ribeiro, P. Lourenço, J. Monteiro, S. Ferreira-Dias, Kinetics of selective adsorption of impurities from a crude vegetable oil in hexane to activated earths and carbons, *Eur. Food Res. Technol.* 213 (2001) 132–138.
- [25] K. Boki, M. Kubo, N. Kawasaki, H. Mori, Adsorption isotherms of pigments from alkali-refined vegetable oils with clay minerals, *J. Am. Oil Chem. Soc.* 69 (1992) 372–378.
- [26] C. Adhikari, A. Proctor, G. Blyholder, Diffuse-reflectance Fourier-transform infrared spectroscopy of vegetable oil triglyceride adsorption on silicic acid, *J. Am. Oil Chem. Soc.* 71 (1994) 589–594.
- [27] M.T. Casford, P.B. Davies, The structure of oleamide films at the aluminum/oil interface and aluminum/air interface studied by Sum Frequency Generation

- (SFG) vibrational spectroscopy and Reflection Absorption Infrared Spectroscopy (RAIRS), *ACS Appl. Mater. Interfaces* 1 (2009) 1672–1681.
- [28] B. Luokkala, S. Garoff, R. Suter, Using x-ray reflectivity to determine the structure of surfactant monolayers, *Phys. Rev. E* 62 (2000) 2405.
- [29] M. Campana, A. Teichert, S. Clarke, R. Steitz, J.R. Webster, A. Zorbakhsh, Surfactant adsorption at the metal–oil interface, *Langmuir* 27 (2011) 6085–6090.
- [30] M.H. Wood, R.J. Welbourn, T. Charlton, A. Zorbakhsh, M. Casford, S.M. Clarke, Hexadecylamine adsorption at the iron oxide–oil interface, *Langmuir* 29 (2013) 13735–13742.
- [31] M. Vuorte, S. Vierros, S. Kuitunen, M. Sammalkorpi, Adsorption of impurities in vegetable oil: A molecular modelling study, *J. Colloid. Interface Sci.* 571 (2020) 55–65.
- [32] S. Lundgren, K. Persson, B. Kronberg, P. Claesson, Adsorption of fatty acids from alkane solution studied with quartz crystal microbalance, *Tribol. Lett.* 22 (2006) 15–20.
- [33] A. Dedinaite, P.M. Claesson, B. Campbell, H. Mays, Interactions between modified mica surfaces in triglyceride media, *Langmuir* 14 (1998) 5546–5554.
- [34] M. Vuorte, S. Kuitunen, M. Sammalkorpi, Physisorption of bio oil nitrogen compounds onto montmorillonite, *Phys. Chem. Chem. Phys.* 23 (2021) 21840–21851.
- [35] J. Zhong, P. Wang, Y. Zhang, Y. Yan, S. Hu, J. Zhang, Adsorption mechanism of oil components on water-wet mineral surface: A molecular dynamics simulation study, *Energy* 59 (2013) 295–300.
- [36] J.L. Bradley-Shaw, P.J. Camp, P.J. Dowding, K. Lewtas, Molecular Dynamics Simulations of Glycerol Monooleate Confined between Mica Surfaces, *Langmuir* 32 (2016) 7707–7718.
- [37] J.L. Bradley-Shaw, P.J. Camp, P.J. Dowding, K. Lewtas, Self-assembly and friction of glycerol monooleate and its hydrolysis products in bulk and confined non-aqueous solvent, *Phys. Chem. Chem. Phys.* 20 (2018) 17648–17657.
- [38] M. Doig, P.J. Camp, The structures of hexadecylamine films adsorbed on iron-oxide surfaces in dodecane and hexadecane, *Phys. Chem. Chem. Phys.* 17 (2015) 5248–5255.
- [39] U. Reimer, M. Wahab, P. Schiller, H.-J. Mögel, Monte Carlo study of surfactant adsorption on heterogeneous solid surfaces, *Langmuir* 21 (2005) 1640–1646.
- [40] T. Zehl, M. Wahab, P. Schiller, H.-J. Mögel, Monte Carlo simulation of surfactant adsorption on hydrophilic surfaces, *Langmuir* 25 (2009) 2090–2100.
- [41] C.M. Wijmans, P. Linse, Surfactant self-assembly at a hydrophilic surface. A Monte Carlo simulation study, *J. Phys. Chem. A* 100 (1996) 12583–12591.
- [42] F. Zheng, X. Zhang, W. Wang, W. Dong, Adsorption and morphology transition of surfactants on hydrophobic surfaces: A lattice Monte Carlo study, *Langmuir* 22 (2006) 11214–11223.
- [43] U. Reimer, M. Wahab, P. Schiller, H.-J. Mögel, Monte Carlo simulation of the adsorption equilibrium of a model surfactant solution on hydrophilic solid surfaces, *Langmuir* 17 (2001) 8444–8450.
- [44] C. Arnold, S. Ulrich, S. Stoll, P. Marie, Y. Holl, Monte Carlo simulations of surfactant aggregation and adsorption on soft hydrophobic particles, *J. Colloid Interface Sci.* 353 (2011) 188–195.
- [45] O.P. Lehtinen, R.W.N. Nugroho, T. Lehtimaa, S. Vierros, P. Hiekkataipale, J. Ruokolainen, M. Sammalkorpi, M. Österberg, Effect of temperature, water content and free fatty acid on reverse micelle formation of phospholipids in vegetable oil, *Colloids Surf. B Biointerfaces* 160 (2017) 355–363.
- [46] W. Chaiyasit, R.J. Elias, D.J. McClements, E.A. Decker, Role of physical structures in bulk oils on lipid oxidation, *Crit. Rev. Food Sci. Nutr.* 47 (2007) 299–317.
- [47] A. Xenakis, V. Papadimitriou, T.G. Sotiropoulos, Colloidal structures in natural oils, *Curr. Opin. Colloid Interface Sci.* 15 (2010) 55–60.
- [48] S. Rangaswamy, I. Sosaku, N. Mitsutoshi, K. Toshinori, M. Takaaki, Characterization of phospholipid reverse micelles in relation to membrane processing of vegetable oils, *Eur. J. Lipid Sci. Technol.* 103 (2001) 93–97.
- [49] F. Valoppi, S. Calligaris, L. Barba, N. Segatin, U.N. Poklar, M.C. Nicoli, Influence of oil type on formation, structure, thermal, and physical properties of monoglyceride-based organogel, *Eur. J. Lipid Sci. Technol.* 119 (2016) 1500549.
- [50] J. Orsavova, L. Misurcova, J.V. Ambrozova, R. Vicha, J. Mlecek, Fatty acids composition of vegetable oils and its contribution to dietary energy intake and dependence of cardiovascular mortality on dietary intake of fatty acids, *Int. J. Mol. Sci.* 16 (2015) 12871–12890.
- [51] E. Yara-Varon, Y. Li, M. Balcells, R. Canela-Garayoa, A.S. Fabiano-Tixier, F. Chemat, Vegetable oils as alternative solvents for green oleo-extraction, purification and formulation of food and natural products, *Molecules* 22 (2017).
- [52] O. Palardy, C. Behnke, L.M. Laurens, Fatty amide determination in neutral molecular fractions of green crude hydrothermal liquefaction oils from algal biomass, *Energy Fuels* 31 (2017) 8275–8282.
- [53] S. Chiaberge, I. Leonardi, T. Fiorani, G. Bianchi, P. Cesti, A. Bosetti, M. Crucianelli, S. Reale, F. De Angelis, Amides in bio-oil by hydrothermal liquefaction of organic wastes: a mass spectrometric study of the thermochemical reaction products of binary mixtures of amino acids and fatty acids, *Energy Fuels* 27 (2013) 5287–5297.
- [54] S. Wang, Q. Wang, X. Jiang, X. Han, H. Ji, Compositional analysis of bio-oil derived from pyrolysis of seaweed, *Energy Convers. Manag.* 68 (2013) 273–280.
- [55] A. Ross, J. Jones, M. Kubacki, T. Bridgeman, Classification of macroalgae as fuel and its thermochemical behaviour, *Bioresour. Technol.* 99 (2008) 6494–6504.
- [56] S. Vierros, M. Sammalkorpi, Phosphatidylcholine reverse micelles on the wrong track in molecular dynamics simulations of phospholipids in an organic solvent, *J. Chem. Phys.* 142 (2015) 094902.
- [57] S. Vierros, M. Sammalkorpi, Role of hydration in phosphatidylcholine reverse micelle structure and gelation in cyclohexane: a molecular dynamics study, *Phys. Chem. Chem. Phys.* 17 (2015) 14951–14960.
- [58] S. Vierros, M. Österberg, M. Sammalkorpi, Aggregation response of triglyceride hydrolysis products in cyclohexane and triolein, *Phys. Chem. Chem. Phys.* 20 (2018) 27192–27204.
- [59] L.K. Shrestha, T. Sato, D.P. Acharya, T. Iwanaga, K. Aramaki, H. Kunieda, Phase behavior of monoglycerol fatty acid esters in nonpolar oils: reverse rodlike micelles at elevated temperatures, *J. Phys. Chem. B* 110 (2006) 12266–12273.
- [60] L.K. Shrestha, M. Kaneko, T. Sato, D.P. Acharya, T. Iwanaga, H. Kunieda, Phase behavior of diglycerol fatty acid esters–nonpolar oil systems, *Langmuir* 22 (2006) 1449–1454.
- [61] L.K. Shrestha, G.R. Shrestha, K. Aramaki, Self-assembled structures of diglycerol monolaurate- and monomyristate in olive oil, *J. Dispersion Sci. Technol.* 30 (2009) 1525–1532.
- [62] F. Peyronel, J. Ilavsky, G. Mazzanti, A.G. Marangoni, D.A. Pink, Edible oil structures at low and intermediate concentrations. ii. ultra-small angle x-ray scattering of in situ tristearin solids in triolein, *J. Appl. Phys.* 114 (2013) 234902.
- [63] R. Gupta, H. Muralidhara, H. Davis, Structure and phase behavior of phospholipid-based micelles in nonaqueous media, *Langmuir* 17 (2001) 5176–5183.
- [64] P.A. Penttilä, S. Vierros, K. Utriainen, N. Carl, L. Rautkari, M. Sammalkorpi, M. Österberg, Phospholipid-Based Reverse Micelle Structures in Vegetable Oil Modified by Water Content, Free Fatty Acid, and Temperature, *Langmuir* 35 (2019) 8373–8382.
- [65] S.H. Tung, Y.E. Huang, S.R. Raghavan, Contrasting effects of temperature on the rheology of normal and reverse wormlike micelles, *Langmuir* 23 (2007) 372–376.
- [66] K. Kittipongpittaya, A. Panya, L. Cui, D.J. McClements, E.A. Decker, Association colloids formed by multiple surface active minor components and their effect on lipid oxidation in bulk oil, *J. Am. Oil Chem. Soc.* 91 (2014) 1955–1965.
- [67] J.H. Harwell, J.C. Hoskins, R.S. Schechter, W.H. Wade, Pseudophase separation model for surfactant adsorption: isomerically pure surfactants, *Langmuir* 1 (1985) 251–262.
- [68] A. Proctor, J. Toro-Vazquez, The freundlich isotherm in studying adsorption in oil processing, *J. Am. Oil Chem. Soc.* 73 (1996) 1627–1633.
- [69] F. Li, L. Katz, Z. Hu, Adsorption of major nitrogen-containing components in microalgal bio-oil by activated carbon: equilibrium, kinetics, and ideal adsorbed solution theory (iast) model, *ACS Sustain. Chem. Eng.* 7 (2019) 16529–16538.
- [70] S. Xu, S.A. Boyd, Alternative model for cationic surfactant adsorption by layer silicates, *Environ. Sci. Technol.* 29 (1995) 3022–3028.
- [71] R.F. Tabor, J. Eastoe, P.J. Dowding, A two-step model for surfactant adsorption at solid surfaces, *J. Colloid Interface Sci.* 346 (2010) 424–428.
- [72] J.M. Mollerup, A review of the thermodynamics of protein association to ligands, protein adsorption, and adsorption isotherms, *Chem. Eng. Technol.* 31 (2008) 864–874.
- [73] I. Lin, P. Somasundaran, Free-energy changes on transfer of surface-active agents between various colloidal and interfacial states, *J. Colloid Interface Sci.* 37 (1971) 731–743.
- [74] M. Zhang, L. Chen, H. Yang, J. Ma, Theoretical study of acetic acid association based on hydrogen bonding mechanism, *J. Phys. Chem. A* 121 (2017) 4560–4568.
- [75] M. Drach, A. Andrzejewska, J. Narkiewicz-Michałek, Theoretical modelling of self assembly of zwitterionic surfactants at the silica/water interface, *Appl. Surf. Sci.* 252 (2005) 730–744.
- [76] R. Johnson, R. Nagarajan, Modeling self-assembly of surfactants at solid-liquid interfaces. ii. hydrophilic surfaces, *Colloids Surf. A Physicochem. Eng. Asp.* 167 (2000) 21–30.
- [77] V. Fainerman, R. Miller, E. Aksenenko, A. Makievski, J. Krägel, G. Loglio, L. Liggieri, Effect of surfactant interfacial orientation/aggregation on adsorption dynamics, *Adv. Colloid Interface Sci.* 86 (2000) 83–101.
- [78] J.G. Fernsler, J.A. Zasadzinski, Competitive adsorption: a physical model for lung surfactant inactivation, *Langmuir* 25 (2009) 8131–8143.
- [79] V. Fainerman, S. Zholob, M. Leser, M. Michel, R. Miller, Competitive adsorption from mixed nonionic surfactant/protein solutions, *J. Colloid Interface Sci.* 274 (2004) 496–501.
- [80] D.J. Tobias, M.L. Klein, Molecular dynamics simulations of a calcium carbonate/calcium sulfonate reverse micelle, *J. Phys. Chem. A* 100 (1996) 6637–6648.
- [81] L.K. Shrestha, M. Dulle, O. Glatter, K. Aramaki, Structure of polyglycerol oleic acid ester nonionic surfactant reverse micelles in decane: growth control by headgroup size, *Langmuir* 26 (2010) 7015–7024.
- [82] S. Vierros, M. Sammalkorpi, Hybrid atomistic and coarse-grained model for surfactants in apolar solvents, *ACS Omega* 4 (2019) 15581–15592.
- [83] V. Vasquez, B. Williams, O. Graeve, Stability and comparative analysis of AOT/water/isoctane reverse micelle system using dynamic light scattering and molecular dynamics, *J. Phys. Chem. B* 115 (2011) 2979–2987.
- [84] T. Kinugasa, A. Kondo, S. Nishimura, Y. Miyauchi, Y. Nishii, K. Watanabe, H. Takeuchi, Estimation for size of reverse micelles formed by AOT and sdehp

- based on viscosity measurement, *Colloids Surf. A Physicochem. Eng. Asp.* 204 (2002) 193–199.
- [85] J.L. Lebowitz, E. Helfand, E. Praestgaard, Scaled particle theory of fluid mixtures, *J. Chem. Phys.* 43 (1965) 774–779.
- [86] J. Talbot, Molecular thermodynamics of binary mixture adsorption: A scaled particle theory approach, *J. Chem. Phys.* 106 (1997) 4696–4706.
- [87] H.S. Ashbaugh, B.A. Pethica, Alkane adsorption at the water–vapor interface, *Langmuir* 19 (2003) 7638–7645.
- [88] M.A. Brusatori, P.R. Van Tassel, A kinetic model of protein adsorption/surface-induced transition kinetics evaluated by the scaled particle theory, *J. Colloid Interface Sci.* 219 (1999) 333–338.
- [89] R.C. Chatelier, A.P. Minton, Adsorption of globular proteins on locally planar surfaces: models for the effect of excluded surface area and aggregation of adsorbed protein on adsorption equilibria, *Biophys. J.* 71 (1996) 2367.
- [90] I. Langmuir, The adsorption of gases on plane surfaces of glass, mica and platinum, *J. Am. Chem. Soc.* 40 (1918) 1361–1403.
- [91] G.R. Parker, Optimum isotherm equation and thermodynamic interpretation for aqueous 1, 1, 2-trichloroethene adsorption isotherms on three adsorbents, *Adsorption* 1 (1995) 113–132.
- [92] K. Vijayaraghavan, T. Padmesh, K. Palanivelu, M. Velan, Biosorption of nickel (II) ions onto *Sargassum wightii*: application of two-parameter and three-parameter isotherm models, *J. Hazard. Mater.* 133 (2006) 304–308.
- [93] S. Kundu, A. Gupta, Arsenic adsorption onto iron oxide-coated cement (IOCC): regression analysis of equilibrium data with several isotherm models and their optimization, *Chem. Eng. J.* 122 (2006) 93–106.
- [94] Q. Jin, L. Huang, A. Li, A. Shan, Quantification of the limitation of Langmuir model used in adsorption research on sediments via site energy heterogeneity, *Chemosphere* 185 (2017) 518–528.
- [95] M. Moreau, P. Valentin, C. Vidal-Madjar, B.C. Lin, G. Guiochon, Adsorption isotherm model for multicomponent adsorbate–adsorbate interactions, *J. Colloid Interface Sci.* 141 (1991) 127–136.
- [96] M.E. Parent, J. Yang, Y. Jeon, M.F. Toney, Z.-L. Zhou, D. Henze, Influence of surfactant structure on reverse micelle size and charge for nonpolar electrophoretic inks, *Langmuir* 27 (2011) 11845–11851.
- [97] M. D. Chatzidakis, K. D. Papavasileiou, M. G. Papadopoulos, A. Xe-nakis, Reverse micelles as antioxidant carriers: an experimental and molecular dynamics study, *Langmuir* 33 (2017) 5077–5085.
- [98] L. K. Shrestha, R. G. Shrestha, K. Oyama, M. Matsuzawa, K. Aramaki, Structural investigation of diglycerol polyisostearate reverse micelles in organic solvents, *J. Phys. Chem. B* 113 (2009) 12669–12679.
- [99] M.E. Leser, L. Sagalowicz, M. Michel, H.J. Watzke, Self-assembly of polar food lipids, *Adv. Colloid Interface Sci.* 123 (2006) 125–136.
- [100] X. Shao, G. Bor, S. Al-Hosayni, S. Salentinig, A. Yaghmur, Structural characterization of self-assemblies of new omega-3 lipids: docosahexaenoic acid and docosapentaenoic acid monoglycerides, *Phys. Chem. Chem. Phys.* 20 (2018) 23928–23941.
- [101] M. Hancer, A. Patist, R. Kean, H. Muralidhara, Micellization and adsorption of phospholipids and soybean oil onto hydrophilic and hydrophobic surfaces in nonaqueous media, *Colloids Surf. A Physicochem. Eng. Asp.* 204 (2002) 31–41.
- [102] G.N. Smith, P. Brown, S.E. Rogers, J. Eastoe, Evidence for a critical micelle concentration of surfactants in hydrocarbon solvents, *Langmuir* 29 (2013) 3252–3258.
- [103] L. Klíčová, P. Sebej, P. Stacko, S.K. Filippov, A. Bogomolova, M. Padilla, P. Klán, Ctab/water/chloroform reverse micelles: a closed or open association model?, *Langmuir* 28 (2012) 15185–15192.
- [104] R. Pichot, R.L. Watson, I.T. Norton, Phospholipids at the interface: current trends and challenges, *Int. J. Mol. Sci.* 14 (2013) 11767–11794.
- [105] N. Kučerka, J.F. Nagle, J.N. Sachs, S.E. Feller, J. Pencic, A. Jackson, J. Katsaras, Lipid bilayer structure determined by the simultaneous analysis of neutron and x-ray scattering data, *Biophys. J.* 95 (2008) 2356–2367.
- [106] G.S. Patil, N.J. Dorman, D.G. Cornwell, Effects of ionization and counterion binding on the surface areas of phosphatidic acids in monolayers, *J. Lipid Res.* 20 (1979) 663–668.
- [107] B. Rai, P. Sathish, J. Tanwar, K. Moon, D. Fuerstenau, et al., A molecular dynamics study of the interaction of oleate and dodecylammonium chloride surfactants with complex aluminosilicate minerals, *J. Colloid Interface Sci.* 362 (2011) 510–516.
- [108] S. Das, F. Khabaz, Q. Nguyen, R.T. Bonnecaze, Molecular dynamics simulations of aqueous nonionic surfactants on a carbonate surface, *J. Phys. Chem. B* 124 (2020) 8158–8166.
- [109] M. Sedghi, L. Goual, W. Welch, J. Kubelka, Effect of asphaltene structure on association and aggregation using molecular dynamics, *J. Phys. Chem. B* 117 (2013) 5765–5776.
- [110] F. Jiménez-Ángeles, A. Khoshnood, A. Firoozabadi, Molecular dynamics simulation of the adsorption and aggregation of ionic surfactants at liquid–solid interfaces, *J. Phys. Chem. C* 121 (2017) 25908–25920.
- [111] N. Yoshii, K. Iwahashi, S. Okazaki, A molecular dynamics study of free energy of micelle formation for sodium dodecyl sulfate in water and its size distribution, *J. Chem. Phys.* 124 (2006) 184901.
- [112] W. Zheng, M.-Y. Tsai, M. Chen, P.G. Wolynes, Exploring the aggregation free energy landscape of the amyloid- β protein (1–40), *Proc. Nat. Acad. Sci.* 113 (2016) 11835–11840.
- [113] S. Bhattacharya, J. Haldar, Thermodynamics of micellization of multiheaded single-chain cationic surfactants, *Langmuir* 20 (2004) 7940–7947.
- [114] M.A. Hoque, S. Mahbub, M.A. Rub, S. Rana, M.A. Khan, Experimental and theoretical investigation of micellization behavior of sodium dodecyl sulfate with cetyltrimethylammonium bromide in aqueous/urea solution at various temperatures, *Korean J. Chem. Eng.* 35 (2018) 2269–2282.
- [115] G. Liu, D. Gu, H. Liu, W. Ding, H. Luan, Y. Lou, Thermodynamic properties of micellization of sulfobetaine-type zwitterionic gemini surfactants in aqueous solutions—a free energy perturbation study, *J. Colloid Interface Sci.* 375 (2012) 148–153.
- [116] J. Van Dalen, K. Van Putte, Adsorptive refining of liquid vegetable oils, *Lipid/Fett* 94 (1992) 567–570.
- [117] A.P. Carpenter, M.J. Foster, K.K. Jones, G.L. Richmond, Effects of salt-induced charge screening on aot adsorption to the planar and nanoemulsion oil–water interfaces, *Langmuir* 37 (2021) 8658–8666.
- [118] J. Määttä, S. Vierros, M. Sammalkorpi, Controlling carbon-nanotube-phospholipid solubility by curvature dependent self-assembly, *J. Phys. Chem. B* 119 (2015) 4020–4032.
- [119] M. Sammalkorpi, A.Z. Panagiotopoulos, M. Haataja, Surfactant and hydrocarbon aggregates on defective graphite surface: Structure and dynamics, *J. Phys. Chem. B* 112 (2008) 12954–12961.
- [120] R. Gibbons, The scaled particle theory for particles of arbitrary shape, *Mol. Phys.* 17 (1969) 81–86.
- [121] X. Zhang, M.J. Borda, M.A. Schoonen, D.R. Strongin, Adsorption of phospholipids on pyrite and their effect on surface oxidation, *Langmuir* 19 (2003) 8787–8792.
- [122] H. Lee, H. Kim, Self-assembly of lipids and single-walled carbon nanotubes: Effects of lipid structure and pegylation, *The Journal of Physical Chemistry C* 116 (2012) 9327–9333.
- [123] M.T. Dronadula, N. Aluru, Phospholipid monolayer/graphene interfaces: Curvature effect on lipid morphology and dynamics, *J. Phys. Chem. B* (2022).
- [124] I. Leontyev, A. Stuchebrukhov, Accounting for electronic polarization in non-polarizable force fields, *Phys. Chem. Chem. Phys.* 13 (2011) 2613–2626.
- [125] I. Leontyev, A. Stuchebrukhov, Electronic continuum model for molecular dynamics simulations of biological molecules, *J. Chem. Theory Comput.* 6 (2010) 1498–1508.
- [126] G. Klesse, S. Rao, S.J. Tucker, M.S. Sansom, Induced polarization in molecular dynamics simulations of the 5-HT₃ receptor channel, *J. Am. Chem. Soc.* 142 (2020) 9415–9427.